2009

Crosslinking of cell-derived 3D scaffolds up-regulates the stretching and unfolding of new extracellular matrix assembled by reseeded cells

Kristopher E Kubow, *James Madison University*
E. Klotzsch
M. L Smith
D. Gourdon
W. C Little, et al.

Published in final edited form as:
Integr Biol (Camb). 2009 December ; 1(0): . doi:10.1039/b914996a.

Crosslinking of cell-derived 3D scaffolds up-regulates the stretching and unfolding of new extracellular matrix assembled by reseeded cells†

Kristopher E. Kubow[‡], **Enrico Klotzsch**, **Michael L. Smith**[§], **Delphine Gourdon**[¶], **William C. Little**, and **Viola Vogel**
Department of Materials, Wolfgang-Pauli-Strasse 10, HCI F 443 ETH Zurich, CH-8093 Zurich, Switzerland, viola.vogel@mat.ethz.ch; Fax: +41 44 632 10 73; Tel: +41 44 632 0887

Abstract

Elevated levels of tissue crosslinking are associated with numerous diseases (cancer stroma, organ fibrosis), and also eliminate the otherwise remarkable clinical successes of tissue-derived scaffolds, instead eliciting a foreign body reaction. Nevertheless, it is not well understood how the initial physical and biochemical properties of cellular microenvironments, stem cell niches, or of 3D tissue scaffolds guide the assembly and remodeling of new extracellular matrix (ECM) that is ultimately sensed by cells. Here, we incorporated FRET-based mechanical strain sensors, either into cell-derived ECM scaffolds or into the fibronectin (Fn) matrix assembled by reseeded fibroblasts, and demonstrated the following. Cell-generated tensile forces change the conformation of Fn in both 3D scaffolds and new matrix over time. The time course by which new matrix fibers are stretched by reseeded cells is accelerated by scaffold crosslinking. Importantly, stretching Fn fibers increases their elastic modulus (rigidity) and alters their biochemical display. Regulated by Fn fiber unfolding, more soluble Fn binds to the native than to the crosslinked scaffolds. Additionally, matrix assembly of fibroblasts is decreased by scaffold crosslinking. Taken together, scaffold crosslinking has a multifactorial impact on the microenvironment that reseeded cells assemble and respond to, with far-reaching implications for tissue engineering and disease physiology.

Introduction

While the significance of the physical characteristics of the microenvironment in controlling cell function and fate is increasingly recognized,[1–5] relatively little is known about the mechanisms by which such physical properties are sensed by cells and how they help to regulate diverse cell functions. For example, it is not well understood how extracellular matrix (ECM) deposited *in vitro* by different cell types can have differential effects on the phenotype of cells that are seeded into it: matrix produced by tumor-associated fibroblasts promotes tumor cell migration,[6] and matrix produced by bone marrow cells prevents the differentiation of mesenchymal progenitor cells.[7] Consequently, efforts to recreate microenvironments characteristic of normal and diseased tissue (*e.g.* fibrotic tissue, cancer stroma, stem cell niches, mesenchyme) in the laboratory, with sufficient fidelity to study

†Electronic supplementary information (ESI) available: Supplementary figures and movies. See DOI: 10.1039/b914996a

Correspondence to: Viola Vogel.

‡Current Address: Department of Cell Biology, University of Virginia, Charlottesville, Virginia, USA
§Current Address: Department of Biomedical Engineering, Boston University, Boston, Massachusetts, USA
¶Current Address: Department of Material Science and Engineering, Cornell University, Ithaca, New York, USA

Conflict of interest statement: The authors declare no competing financial interests.

diseases and test therapies on the cellular level, has proved a complex undertaking and exposed gaps in our understanding of cell–microenvironment interactions.[8–10] Likewise, synthetic strategies for mimicking the natural extracellular environment for applications in tissue engineering and regenerative medicine have yielded few scaffolds that are able to regenerate functional soft tissues successfully. Possibly the most promising tissue scaffolds today are not in fact artificial, but de-cellularized ECM derived from tissue.[11] Even de-cellularized rat hearts, reseeded with cells and exposed to simulated pulsatile flow and electrical stimulation, could regain partial pump function after eight days.[12] Clinically, tissue-derived ECMs have been successfully used as scaffolds and grafts for the reconstruction of tendons, arteries, and numerous other soft tissues;[11] however, the properties that enable these ECMs to successfully guide tissue regeneration are still relatively uncharacterized. It is also poorly understood why chemically crosslinking tissue-derived scaffolds in order to enhance their mechanical stability typically results in chronic inflammation and fibrous encapsulation rather than tissue regeneration.[13,14] More generally, enhanced ECM crosslinking *via* natural processes, while a critical process in wound healing, is also associated with the pathologies of numerous diseases.[15–17] For example, lysyl oxidase, an enzyme that crosslinks collagen and elastin, is up-regulated in fibrosis, but down-regulated in malignant cells.[18]

How does crosslinking affect the ECM microenvironment, and thereby cell and tissue function? Both the biochemical composition and the physical properties of the cellular microenvironment control numerous cellular processes, including cell differentiation,[1,2,4,7,19] and tumor cell development and metastasis.[3,5,6,20–22] Initial interactions between cells and 2D substrates are dependent, for example, on substrate rigidity, topography and ligand presentation (as reviewed in ref. [23–28]). Later events such as stem cell proliferation and differentiation can be influenced by the conformation of surface-adsorbed fibronectin (Fn)[29,30] as well as substrate rigidity.[4] In all of these experiments, initial surface characteristics were correlated with cell phenotype, yet the molecular mechanisms by which these initial substrate parameters direct long-term cell fate remain unknown. Indeed, it has long been known that a state of dynamic reciprocity exists in which signals from the microenvironment affect cell behavior and cells modify their microenvironment by, for example, ECM deposition and degradation.[31] Given that many cell types begin to assemble their own matrix soon after being seeded onto a surface or 3D scaffold, the question arises whether late cell phenotypes are primarily directed by the initial contact or by the evolving properties of the microenvironment. This lack of knowledge is partially due to the fact that tools were not available that enabled the monitoring of changes in the microenvironment's physical properties in the context of a 3D matrix. In 2D culture, traction forces that cells apply to their microenvironment in early phases have been probed using microfabricated substrates[32,33] and the rigidity of matrix that surrounds cells cultured on planar surfaces has been measured by indentation measurements using an AFM tip.[34,35]

By exploiting a fluorescence resonance energy transfer (FRET)-based method that utilizes FRET-labeled Fn as a mechanical strain sensor,[36–38] we have previously shown that Fn strain and unfolding in matrix produced *de novo* by fibroblasts on 2D glass surfaces is not static, but gradually increases as cells apply force and deposit new Fn fibers. Here, we probed for the first time how cells that are reseeded into a cell-derived 3D scaffold remodel the scaffold and, in response to the scaffold cues, gradually build-up their new matrix environment. By incorporating FRET-labeled Fn, either into cell-derived ECM scaffolds or into the Fn matrix assembled by reseeded fibroblasts, we asked here how crosslinking of the scaffolds affected their characteristics and those of newly assembled Fn fibers during cell-mediated remodeling over time. Recent findings have indicated that cell-generated traction forces are sufficiently high to stretch[39,40] and unfold fibrillar Fn.[37,41,42] Moreover, force-induced unfolding of the secondary structure of intra- and extracellular proteins has been

implicated in the conversion of a mechanical stimulus to a change in protein functionality and/or biochemical signaling.[43–48] Previously, we have shown in 2D that the amount of Fn stretching and unfolding is up-regulated by the rigidity of a polymeric 2D substrate against which the cells pull.[42] However, mounting evidence indicates that observations made in 2D cell culture are not necessarily transferable to 3D.[8,9] For example, cells on 2D substrates *versus* 3D matrices have a different morphology and adhesion structure,[49–51] show differences in cell motility,[52,53] and favor different non-muscle myosin II isoforms for force application.[54] The molecular strain or force-induced elongation of a molecule directly reads-out the extent to which structural, and thus potentially functional, alterations have occurred.[47] Yet, to our knowledge, there is no information about how the mechanical strain of newly assembled matrix relates to the rigidity of a provided 3D scaffold.

As cells pull locally on individual ECM Fn fibers, at least two important fiber parameters are altered: fiber rigidity (kPa to MPa)[55] and Fn structure.[37,41,47] To our knowledge, no work has made a systematic attempt to identify which cellular functions are regulated either by Fn fiber rigidity, or by stretch-sensitive protein conformations. Here, we differentiate between these two causes by comparing cellular responses to cell-derived 3D scaffolds, and to one-dimensional Fn fibers in a stretched or relaxed conformation. Cell-derived matrices were used as our primary model system, since they are well characterized with respect to cell–matrix interactions.[7,20,34,49,52,56,57] Moreover, FRET-labeled Fn, added to the culture medium, can be harvested by cells and incorporated into the ECM to directly report force-induced changes in Fn conformation.[36,37] Thus the mechanical strain caused by cell traction forces can be mapped either in 3D cell-derived scaffolds or in the newly assembled Fn fibers. Chemically crosslinking of the scaffold allows us to address the differential roles of rigidity and Fn conformation, since it increases fiber rigidity while locking-in the more relaxed protein conformation of the de-cellularized scaffold. In the second part of our study we use a simplified, but more-controlled, model system using manually deposited Fn fibers with tunable rigidity and Fn conformation in order to dissect the causes for the observations made in the cell-derived ECMs. Chemical crosslinking has previously been employed to enhance the mechanical stabilization of tissue-derived scaffolds, yet with adverse clinical outcomes.[13,14] We thus limited our studies here to chemical crosslinking, but later discuss the extension of our findings to crosslinking *via* natural biochemical pathways, as occurs in wound healing and diseases.

Results

To grow cell-derived ECM scaffolds, NIH 3T3 fibroblasts were cultured for four days on glass and allowed to assemble soluble Fn into matrices that grew to approximately 17 μm thick. The ‘four-day’ matrices were then de-cellularized using an alkaline detergent solution. Similar to previous studies,[20,56] the fibrillar structure of the de-cellularized matrices was preserved and their final thickness was about 10–15 μm. When needed, the de-cellularized matrices were subsequently crosslinked with 4% formaldehyde. There are numerous chemical compounds and non-chemical methods that have been used to crosslink tissue engineering scaffolds for medical applications,[58] including formaldehyde and glutaraldehyde (*e.g.* ref. [13]). Both chemicals have been used previously to study the effects of ECM rigidity on cell behavior[49,56] and both increase Fn matrix rigidity by similar amounts;[34] however, glutaraldehyde is autofluorescent. Therefore, formaldehyde was used in our studies as a model crosslinking chemical.

The native and crosslinked de-cellularized ECM scaffolds were reseeded with fibroblasts and imaged over 48 h to study how they were remodeled, and served as a framework for the assembly of new matrix. Since cells can harvest Fn from the cell culture medium and incorporate it into their own ECM fibers, adding trace amounts of donor/acceptor-labeled Fn

(Fn-DA) allows live-cell imaging of the Fn matrix dynamics[37,42] and mapping of the corresponding mechanical strains.[38] To probe the mechanical reciprocity between old and new matrix, the cells were allowed to incorporate trace amounts of Fn-DA either into the 3D scaffold or the newly assembled matrix and the live cell cultures were then spectroscopically analyzed. Due to the large size of Fn, the best mechano-sensitivity was obtained when Fn was labeled with multiple fluorophores: the four buried cysteines of the Fn dimer (modules $FnIII_7$ and $FnIII_{15}$) were labeled with acceptors, and approximately seven donors were conjugated randomly to lysines (Fig. 2a).[37] Dilution of Fn-DA with an excess of unlabeled Fn prevented intermolecular FRET.[37]

Fibroblasts invade the cell-derived scaffolds upon reseeding

Reseeded fibroblasts invaded the scaffolds by pushing fibers near the cell perimeter outwards and fibers underneath the cell downwards (Fig. 1a). The fibers surrounding the invading cells were progressively stretched and, in the native scaffolds, were compacted to form transient fibrous ring structures (arrows). Regardless of crosslinking, the cells typically resided (Fig. 1b) near the top of the scaffold, with the nucleus and sometimes part of the cell body exposed (cells 1 and 3) or near the bottom of the matrix with some parts of its ventral side or pseudopodia touching the surface (cell 2). The position of the cell in the scaffold did not appear to alter its morphology or behavior.

After invading the scaffolds, the cells began to migrate by grabbing distant matrix fibers with their pseudopodia and pulling their body forward while at the same time deforming the anchoring fibers. Obstructing fibers were pushed out of the way to accommodate the cell body (Fig. 1c and Supplementary Movie 1[†]). Once the cells had passed, the local matrix fiber deformations relaxed back, although not necessarily to the same position. When the fibers in front of the cell body were parallel to the direction of movement, there was little permanent fiber rearrangement (Supplementary Movie 2[†]). These behaviors were not altered in crosslinked scaffolds, although overall fiber movement was reduced (Supplementary Movie 3[†]). The presence of broad-spectrum protease and matrix metalloproteinase inhibitors did not affect the mode of cell migration (data not shown).[59]

Using FRET to measure Fn strain (extension) caused by cell-generated tensile forces

While *in situ* force sensors have been available for several years,[32,35,60] it is important to recognize that it is not the force that directly defines whether a molecular binding site is altered, but the molecular structure as distorted by tensile forces (mechanical strain). The advantage of FRET is that it directly probes the average increase of donor–acceptor distances and is thus sensitive to mechanical strain.[37] Since the acceptors are located on modules $FnIII_7$ and $FnIII_{15}$, it is important to note that we were probing only the force-induced structural changes in the proximity (<12 nm) of these acceptors, as indicated by yellow spheres in Fig. 2a. The peak intensities of the acceptor and donor fluorophores were measured using spectral confocal microscopy (not correcting for residual cross-talk between the excitation and emission channels). The resulting intensity ratios, I_A/I_D, of the ECM fibrils are given as histograms (Fig. 2d and f), or spatially resolved as false-colored images (Fig. 2b and c). In order to associate the intensity ratios derived from ECM fibrils to structural alterations, they were compared to those obtained from soluble Fn-DA denatured in known concentrations of guanidine HCl (GdnHCl),[37] or from individual Fn fibers in conjunction with stress–strain measurements (Fig. S1 in the ESI[†] and ref. [55]). Previous work has demonstrated that Fn in solution begins to lose its secondary structure in GdnHCl concentrations higher than 1 M, and is completely denatured in 4 M GdnHCl (ref. [37]). Moreover, the intensity ratio measured at 1 M GdnHCl correlates well with the intensity

[†]Electronic supplementary information (ESI) available: Supplementary figures and movies. See DOI: 10.1039/b914996a

ratio below which we see a large increase of Fn unfolding in single freely suspended Fn fibers (approximately 150–200% strain).[55] The 1 M GdnHCl denaturation curve point, which roughly corresponds to 200% strain (three-fold extension), was measured using Fn monomers in order to prevent additional FRET caused by crossover of the dimer arms.

Fn fibers partially contract when the ECM is de-cellularized

Four-day ECMs, labeled with Fn-DA, were prepared, imaged before and after de-cellularization, and then 18 and 48 h after reseeding in order to map force-induced local alterations of Fn's structure. Representative slices from the confocal z-stacks of four-day and de-cellularized scaffolds are shown in Fig. 2b and c. There was no statistically significant difference in the intensity ratio between slices taken at different z-positions (data not shown).

Four-day matrices had an average median intensity ratio of 0.52 that shifted up to 0.57 upon de-cellularization. De-celullarization eliminated cell-generated matrix tension and thus allowed the ECM fibers to partially contract, as indicated by FRET recovery. The associated increase in FRET intensity ratio is clearly seen in the color shift from green-blue to yellow in the images (Fig. 2b and c) and in the right-shift of the corresponding histograms (Fig. 2d and f). FRET recovery was, however, not complete, indicating that the refolding of at least a fraction of Fn molecules might be inhibited by interactions with other tightly bound proteins. The de-cellularization procedure occasionally caused the matrix to tear or partially detach from the substrate. Damaged matrices were detected by visual inspection and by their very high FRET,[37] and were excluded from the analysis.

To estimate the partial loss of secondary structure that occurs in the proximity of the acceptor sites, the percentage of pixels in the FRET histograms with intensity ratios less than those obtained for the Fn monomer in 1 M GdnHCl solution is shown as shaded regions (Fig. 2d and f), and is summarized for multiple experiments in the bar graph (Fig. 2e). Elsewhere, we show by straining freely suspended single Fn fibers, that massive exposure of the cryptic cysteines buried in modules $FnIII_7$ and $FnIII_{15}$ begins at a strain of 150% (ref. [55]). The FRET ratios measured at this point on single Fn fibers correlated with those obtained for soluble monomeric Fn molecules in 1 M GdnHCl solution.[55] De-cellularization of four-day old cell-derived matrices caused the percentage of fibers with perturbed secondary structure, to decrease from 82 to 61% ($p < 0.05$; Fig. 2e). These results agree with previous studies showing that the elimination of cell-generated tensile forces leads to partial matrix relaxation.[37,42,61]

Native 3D scaffolds are progressively stretched and unfolded over the course of days by cell-generated tensile forces whereas crosslinked scaffolds are not

Rigidifying Fn-based ECMs *via* chemical crosslinking affects cell migration,[56] causes changes in the molecular composition of cell adhesion sites[49] and increases the force necessary to detach cells from the matrix.[34] We therefore asked if native and crosslinked scaffolds would experience differences in the time-course of remodeling. During the 48 h after reseeding, the fibroblasts progressively stretched the native scaffold fibers, which can be seen graphically in the change of the color-coded images in Fig. 2c and 3a,b from yellow-green (0 h) to green-blue (48 h) (corresponding histograms and controls can be found in the ESI, Fig. S2 and S3[†]). FRET revealed, however, that crosslinked scaffolds were not stretched during the 48 h of cell-mediated remodeling (Fig. 2c and 3c,d). While cells increased the percentage of partially unfolded fibers in native scaffolds from roughly 61 to 91% over the course of 48 h ($p < 0.05$), the strain of crosslinked scaffolds was not significantly altered (64% at 48 h, Fig. 3i).

To gain insight into how the alterations of the FRET ratios related to the average extensions of the ECM fibers, corresponding uniaxial, single fiber strains are shown on the far right side of Fig. 3i ("Single Fiber Measurements"). This FRET–strain correlation was deduced from a separate experiment using freely suspended Fn fibers.[55] Crosslinking thus locked-in a more relaxed conformation of fibrillar Fn, corresponding to an average strain of around 200% that remained unchanged over time. In contrast, the Fn fibers of the native scaffold were stretched from about 200 to 300% strain over 48 h.

New fibers in crosslinked scaffolds have an altered morphology and become stretched more rapidly

Because newly deposited matrix plays a prominent role in defining the properties of the cellular microenvironment,[62] we asked how crosslinking the scaffolds would affect the deposition and conformation of new Fn fibers. Once seeded, the fibroblasts assembled new (Fn-DA-labeled) fibers throughout the full thickness of (unlabeled) native and crosslinked scaffolds. Similar to previous studies,[42,56] the new fibers deposited on native scaffolds closely followed and co-localized with the existing matrix fibers, although some non-overlapping fibers were also observed (Fig. 4a–c, arrows). In contrast, when the scaffolds were crosslinked, the new fibers did not co-localize with the existing fibers, although they were anchored to them and aligned in the same general direction (Fig. 4e–g).

Significantly, the newly deposited Fn fibers in the native scaffolds, which were initially soft, showed little unfolding (approximately 100% strain, Fig. 3e and i), but were slowly stretched over 48 h as the cells actively remodeled their environment. From 18 to 48 h, the percentage of Fn with partial unfolding, as deduced from the FRET histograms, increased from 17 to 46% (Fig. 3i). Crosslinking of the scaffold had a major impact on the physical state of newly assembled ECM: the new Fn fibers deposited in crosslinked scaffolds were already highly stretched after 18 h with little further stretching as time progressed (Fig. 3g and h). They exhibited percent-partial-unfolding levels similar to those found in new ECM deposited by fibroblasts directly on glass (Fig. 3i). Thus, Fn fibers assembled by fibroblasts on crosslinked scaffolds were initially more unfolded than on native scaffolds, but by 48 h, they exhibited similar conformations. Based on previous work showing that cells on rigid 2D substrates generate more highly stretched Fn fibers than on soft 2D surfaces[42], our results suggest that—at least initially— the cells in the crosslinked 3D scaffold were experiencing a far more rigid microenvironment and respond to it by increasingthe stretching of new ECM.

Stress–strain measurements to quantify how chemical crosslinking increases the rigidity of single Fn fibers

Earlier studies have shown that chemical crosslinking increases ECM rigidity enough to change cell behavior,[49,56] and that cells can sense a wide range of elastic moduli.[4,24,63] A study has recently used AFM nano-indentation to measure the increase in overall ECM rigidity due to crosslinking;[34] however, we were interested in measuring the mechanical properties of individual Fn fibers to better understand how chemical crosslinking impacts the quantitative relationship between stress–strain characteristics and functionality. Because the cell-derived scaffolds had a broad distribution of thicknesses and spatiotemporal variations in strain, we performed our measurements on isolated, manually produced fibers that were more controlled with regard to these variables. We manually pulled Fn fibers from a droplet of concentrated Fn solution.[38] The fibers were deposited across and attached to microfabricated PDMS ridges, and then rehydrated to enable force-extension measurements on freely suspended fibers in physiological buffer (Fig. 5a). Pulling Fn fibers out of a droplet requires > 10 μN of force and results in fibers with 140% pre-strain.[55] Therefore, in order to relax the fibers to their fully relaxed state, the fibers were deposited on PDMS ridges that

were pre-strained in a one-dimensional strain device; then the PDMS ridges, along with the fibers, were relaxed until fiber buckling was observed. Multiple, independent stress–strain measurements were performed on single fibers before and after crosslinking with 4% formaldehyde using a MEMS actuator and force sensor.[64] As the tip advanced, the MEMS device measured the force acting on the tip while the fiber length and fiber diameter were monitored by confocal microscopy (Fig. 5b and c). The stress is the force normalized per unit cross-sectional area of the Fn fiber, and the fiber strain is given by $(l-l_0)/l_0*100\%$, where l is the fiber length when stretched and l_0 is length of the relaxed fiber. The Elastic or Young's Modulus is given by the slope of the stress–strain curve (see Materials and Methods). A detailed discussion of this technique is published elsewhere.[55]

Fig. 5d shows the force–strain curve for a representative fiber before and after crosslinking, as well as the stress (Fig. 5e) and Young's Modulus (Fig. 5f; data from additional fibers in the ESI, Fig. S4[†]). The force needed to strain the fibers was several-fold higher after crosslinking. For the representative fiber shown in Fig. 5, a strain of 80% required a force of 1.7 μN, whereas after crosslinking, a force of 5.5 μN was required (Fig. 5d). While Fig. 5 shows that the crosslinked Fn fibers are extensible, cell-generated forces did not seem to be sufficient to stretch them within the sensitivity of our FRET technique (Fig. 3). Note that the force needed to stretch a fiber is proportional to its cross-sectional area, which was approximately 7 μm^2 for our manually pulled Fn fibers and therefore much larger than that of cell-made fibers. For example, the thinnest known Fn fibers are 10–12 nm in diameter[65,66] and would only require 19–27 pN of force to achieve an 80% strain. While cells typically apply forces of a few nN per square micrometer of adhesion area,[67] the forces cells apply to adhesions smaller than 1 μm^2 can be considerably higher.[32]

The slope of the stress–strain curves for Fn fibers is not constant, unlike many linear elastic materials whose elasticity can be approximated by a single elastic spring model (Hooke's law). The Young's Modulus increases steadily as the fibers are stretched (Fig. 5f). Crosslinking the fibers also increased their rigidity (Young's Modulus) from 0.8 to 2.0 MPa for 0–50% strain (median values; $p < 0.01$, $n = 8$, paired t-test). For crosslinked fibers, only strains up to 200% are shown because these rigid fibers detached from the ridges under high force prior to their breakage. Taken with our earlier finding that cells are not able to cause detectable conformational changes in crosslinked scaffolds, these data imply that cell-generated forces are not high enough to stretch the fibers sufficiently to cause a detectable change in Fn conformation.

Soluble Fn binding is up-regulated by stretching individual Fn fibers and is not affected by crosslinking

Does crosslinking affect the binding of proteins to Fn fibers and the mechanosensitive exposure of cryptic sites upon stretching? In particular, the cryptic self-association site located in Fn module III_1 is known to be exposed by cell-generated strain and is involved in fibrillogenesis.[46,68] We therefore asked if soluble Fn would bind to Fn fibers in a conformation-dependent manner and whether chemical crosslinking of the pre-strained fibers would affect this process. Again, because of the inherent variability of Fn fibers in cell-derived scaffolds, we used manually deposited fibers with controlled levels of strain.

Fn fibers containing Fn-DA were deposited in an asterisk pattern on a thin silicone sheet so that when one-dimensional strain was applied, a range of conformations was obtained (Fig. 6b and e).[38] The stretched fibers were then either crosslinked or used in their native state. After incubating the fibers with soluble Fn-Cy5, the intensities of the bound Fn-Cy5 were measured at each pixel (Fig. 6c and f). Fig. 6a and d show Fn-Cy5 intensities on fibers with different conformations and demonstrate that the binding of soluble Fn increased with fiber strain, regardless of crosslinking. Nevertheless, our previous experiments showed that cell-

generated forces were not able to stretch crosslinked Fn fibers sufficient to change their conformation, resulting in less partial unfolding in the crosslinked scaffolds (Fig. 3i). Taken together, our data imply that the binding of soluble Fn to fibrillar Fn is up-regulated in native but not in crosslinked scaffolds due to the limited force cells can apply to matrix fibers.

The conformation of newly assembled Fn fibers does not correlate with the conformation of older fibers

In our earlier experiments, the crosslinked cell-derived scaffolds provided a 3D microenvironment with relatively constant high rigidity and relaxed Fn conformation, while the rigidity and level of Fn unfolding in the native scaffold began low and increased over time (Fig. 3i). Although we hypothesized that the difference in conformation of the Fn matrix, newly deposited on the native and crosslinked scaffolds (Fig. 3e, g and i), was an effect of the elevated rigidity of the crosslinked scaffold, we could not exclude the possibility that it was an effect of a difference in the scaffolds' Fn conformation. This could be due, for example, to structural templating or due to a Fn-conformation-dependent change in outside-in cell signaling. In order to determine if the Fn conformation in existing fibers affected the conformation of newly deposited fibers, we studied the matrix assembled by cells seeded onto single Fn fibers with an adjustable conformation and constant rigidity. The manually deposited fibers provided a more controlled system than the 3D cell-derived scaffolds and, although the two model systems were different in many respects, a recent study has shown that cell migration in a one-dimensional environment mimics many of the characteristics of migration in a 3D environment.[52]

Individual Fn fibers were manually deposited on silicone sheets in a one-dimensional strain device, and either relaxed to an absolute strain of 56%or stretched to 500%(high unfolding; ESI, Fig. S1D[†]). The rigidities of single Fn fibers tightly physisorbed to silicone sheets were all in the range of a few MPa (Fig. 5f).[55] Since it has been previously shown that NIH 3T3 cells are not sensitive to increases in the rigidity of 2D substrates beyond the order of 10 kPa,[63,69] we conclude that the cells sensed a similar rigidity on the surface-attached native and crosslinked fibers.

After 18 h culture time, most of the cells remained solely in contact with the manually deposited fiber (Fig. 7a, i and ii) and had generated a Fn matrix (Fig. 7a, iii). Cells with pseudopodia contacting the BSA-blocked silicone surface were not analyzed. Cell-generated Fn fibers were attached to the manually deposited fiber (Fig. 7a, iv, arrows) and, at higher focal planes, wrapped around the cells (Fig. 7a, v, arrows). There was no statistical difference between the median intensity ratios of new matrix deposited on stretched and relaxed fibers (Fig. 7b). Moreover, there were no noticeable differences in cell or matrix morphology, and no significant differences in cell and matrix density between stretched and relaxed fibers (unpublished data). Taken with our earlier findings, this indicates that the cells primarily responded to the rigidity of the Fn fibers that were bound to the silicone sheets, rather than to the Fn conformation of stretched *versus* relaxed fibers.

Discussion

Once cells are seeded onto a material, or into a 3D scaffold, they soon begin to assemble their own ECM, and will ultimately sense and respond to the new ECM fibers that surround them, and to which they are attached. While many studies have correlated how initial material properties correlate with cell fate at late time points,[4,5,30,70] little information is available about how the properties of the microenvironment change over time. Seldom addressed is the role played by newly deposited matrix, much less how the properties of the new matrix are guided by those of the pre-existing matrix, scaffold or biomaterial. In an

effort to shed light into the underpinning mechanisms, we made the following observations. Firstly, by applying local traction forces to the ECM, cells regulate the rigidity and biochemistry (Fn conformation) of their microenvironment in a time-resolved manner (Fig. 3, 5 and 6). Secondly, the physical and biochemical characteristics of newly deposited Fn depend on the rigidity of the pre-existing Fn scaffold (Fig. 5 and 7). Thirdly, chemical crosslinking an ECM-based scaffold changes the time-course of the cell-mediated remodeling, not only of the scaffold, but also of the newly deposited Fn matrix (Fig. 3). Long-term cell fate might be impacted by the fact that traction forces cause a gradual increase in rigidity, which correlates with an increase in the average unfolding of Fn in both old and new ECM fibers. The stretching of fibers up-regulates the binding of soluble Fn (Fig. 6), which could at least in part be due to the exposure of cryptic sites on FnIII modules involved in regulating Fn fibrillogenesis.[38,46,47,71] Thus, the timedependent changes in Fn conformation observed in the scaffolds and in the newly deposited matrix directly alter the physical as well as the biochemical properties of a cell's microenvironment, with the potential to switch outside-in cell signaling events.[25,44,72] It has already been demonstrated that different conformations of surface-adsorbed, non-fibrillar Fn can impact cell differentiation.[29,30,73]

In light of the aforementioned studies that demonstrated adverse host responses associated with the crosslinking of tissue-derived scaffolds,[13,14] we showed here that crosslinking of a cell-derived 3D scaffold increases the rigidity (Fig. 5f) and locks-in the conformation (Fig. 3i) of the scaffold, at least in the regime of forces that cells can apply to scaffold fibers. Most significantly, scaffold crosslinking profoundly affects specific characteristics of newly-assembled ECM. Crosslinking the cell-derived 3D scaffolds greatly accelerated the rate at which reseeded fibroblasts stretched and unfolded fibrillar Fn in their newly assembled matrix (Fig. 3i, closed squares), but decreased the amount of new matrix deposited (Fig. 3f and h). Using manually deposited Fn fibers with a controlled Fn conformation and constant rigidity, it was furthermore shown that the increased scaffold rigidity—not the locked-in, relaxed conformation—caused the reseeded cells to apply higher tensile forces at earlier time-points (Fig. 7b). The differences in the time-course of Fn unfolding between the native and crosslinked scaffolds, and the new matrix deposited therein, imply, as elaborated earlier, that cell-generated forces cause major differences in the physical and biochemical properties of new ECM fibers, which define the cellular microenvironment. Future research is needed to reveal more about the mechanisms of how ECM stretching might regulate certain outside-in cell signaling events and ultimately cell fate.[48,74]

Although it was beyond the scope of this study, naturally occurring ECM crosslinkers exist that alter cellular microenvironments during wound healing and in disease, and thereby direct cell phenotype. Crosslinks, regardless of their origin, cause an increase in mechanical stability. A recent study has demonstrated that the rigidity of Fn ECM is increased to a similar extent by treatment with formaldehyde, glutaraldehyde or factor XIIIa transglutaminase.[34] Biological crosslinking enzymes such as the transglutaminases[15] and lysl oxidase[18] and naturally occurring crosslinks such as advanced glycation end products[16,17] are associated with tissue stiffening in wound healing, and in diseases such as atherosclerosis and cancer. It is now well appreciated that microenvironment rigidity can guide cell phenotype. For example, the stiffening environment of the provisional matrix of a wound promotes differentiation of fibroblasts to myofibroblasts[75] and a rigid ECM can promote a malignant phenotype.[5] Future studies need to determine to what extent altered Fn deposition and strain-dependent alterations in conformation and rigidity play a role in determining cell phenotype in disease, and the maintenance of homeostasis.

Conclusion

In conclusion, we show for the first time to our knowledge that major time-dependent changes occur in the physical and biochemical properties of the cellular microenvironment, which consists of the 3D scaffold and the newly assembled matrix. The time-course by which newly assembled matrix changes its physical and biochemical properties, and the effects of scaffold properties need to be considered if one aims to decipher the molecular mechanisms by which microenvironment properties control cell phenotype. For example, the time required for an environmental stimulus (*e.g.* rigidity, Fn conformation) to determine cell lineage can vary between hours and weeks depending on the cell type and stimulus,[4,29] yet how intermediate events regulate the late outcome is unknown. Proper consideration of how cell-generated forces alter the immediate cellular microenvironment as function of time is important not only in the design of tissue scaffolds but also to decipher how matrix biology directs long-term changes in cell and tissue phenotype.

Materials and methods

Fn isolation, fluorescent labeling, and chemical denaturation curves

Fn was isolated, labeled, and calibrated in GdnHCl (ESI, Fig. S1[†]) as previously described.[37] Fn was isolated from human plasma (Zürcher Blutspendedienst SRK, Switzerland) by affinity chromatography. Fn was doubly labeled with Alexa Fluor 488 (donor) on amines and Alexa Fluor 546 (acceptor) on free sulfhydryls. The two batches of Fn-DA used in this study had an average of 7 donors and 3.5 acceptors per molecule. Singly labeled Fn was labeled on amines with Alexa 488, Alexa 546, Alexa 633 or Cy5. Labeled Fn was always used with an excess of 90–95% unlabeled Fn to prevent intermolecular energy transfer between molecules within a fiber. All dyes were from Molecular Probes (Invitrogen).

Manually deposited fibers, the strain calibration curve, and soluble Fn binding assay

Manually deposited fibers were deposited on silicone sheets and strained on a custom-made, one-dimensional strain device as previously described.[38] Briefly, 0.25 mm-thick silicone sheets (Specialty Manufacturing, Saginaw, MI) were cut into a dog-bone shape and cleaned by sonication in 2% PCC-54 (Sigma-Aldrich) and then 70% ethanol. A 300–500 μg ml^{-1} Fn solution (5% Fn-DA, 95% unlabeled) was deposited as a small drop on the silicone sheet. Fibers were pulled from the drop with a sharp tip and deposited onto the silicone sheet. Afterwards, the drop was aspirated and the sample washed with 2% (w/v) BSA in PBS, and soon thereafter immersed in PBS buffer for all further studies. Fiber strain was calculated from the macroscopic strain of the silicone sheet.[37]

For the binding assay of soluble Fn (Fn-Cy5) to stretched Fn fibers (Fn-DA), the Fn fibers deposited on silicone sheets were either crosslinked with 4% formaldehyde (EM grade; Polysciences, Inc.) in PBS for 1 h or used in their native state. After blocking with 4% BSA for 15 min., the fibers were incubated with 10 μg ml^{-1} Fn-Cy5 in 4% BSA in PBS for 20 min. at room temperature. After rinsing with PBS, donor, acceptor and Fn-Cy5 intensities were measured at each pixel. The Fn-Cy5 images were smoothed using a 3 × 3 pixel sliding averaging filter, and then the PMT background noise was subtracted. The Fn-Cy5 intensities were normalized to account for differences in protein mass by dividing each pixel's intensity by the sum of the peak donor and acceptor intensities (with 488 nm excitation) at the same pixel. This normalization method gives equivalent results to normalizing against the fluorescence of singly labeled Fn fibers (D.G., unpublished data).

Mechanical measurements of manually deposited fibers

Arrays of PDMS ridges were made using standard photolithography and PDMS replica molding. The master replica was then cast into a thin film of PDMS (1 : 10 curing agent to pre-polymer) on the aforementioned silicone sheets. The trenches between the ridges were 50–500 μm wide, about 20 μm deep and >400 μm long. To enable covalent crosslinking of the manually deposited fibers to the tops of the trenches, the structures were first treated with air plasma (250 mbar, 1 min.), then with 3% 3-aminopropyldimethyl-methoxysilane (ACROS Organics) in deionized water for 20 min, and finally with 0.5% glutaraldehyde (Sigma-Aldrich) in water for 30 min. Glutaraldehyde is a simple bi-functional crosslinker, so this procedure resulted in the glutaraldehyde binding with one aldehyde group to the PDMS ridges and presenting the other (active) group to allow covalent attachment of the Fn fiber. The substrates were rinsed with deionized water to remove unreacted glutaraldehyde and dried. The substrates were then pre-strained with the 1D strain device, and Fn fibers were manually deposited across the trenches. The parts of the Fn fibers in contact with the ridges became covalently linked to the PDMS *via* the free aldehyde groups. The samples were then relaxed until the first signs of fiber sagging into the microfabricated trenches were noticed, indicating that the fibers were fully relaxed. Since the fibers spanned multiple trenches, it was possible to measure each fiber independently in multiple locations, before and after crosslinking. Fibers were crosslinked with 4% formaldehyde for 1 h at room temperature, then incubated for 3 h in PBS before being measured again.

The 3-axis micromanipulator (Sutter MP-285) with an attached custom-made MEMS force sensor[64] was mounted to the stage of a confocal microscope (Olympus FV1000; 40×, 0.90NA, water-immersion objective). The micromanipulator advanced the MEMS device at a constant velocity as controlled by a computer. Because the tip deffected in response to resistive force, it did not proceed with a constant velocity and thus fiber strain was measured from images taken with the confocal microscope. The force on the tip (F) was corrected to yield the tensile force on the fiber (f) using the following equation (x, extension).

$$f = \frac{F}{2\sqrt{1 - \frac{1}{x^2}}}$$

The stress was calculated from the measured force values by dividing by the fiber's cross-sectional area, which was assumed to be constant over all measured strains.[55] The cross-sectional area was measured from confocal images by averaging the full-width-at-half-maximum of the fiber measured at five different locations. The elastic modulus at a given strain was calculated by dividing the change in stress by the change in strain between the data points two-before it and two-after it.

Cell culture and membrane staining

NIH 3T3 fibroblasts (American Type Culture Collection, ATCC) were cultured in DMEM (ATCC) supplemented with 10% newborn calf serum (Gibco, Invitrogen) in a humidified incubator at 37 °C with 5% CO_2. During experiments, the medium contained 1% penicillin–streptomycin–fungizone (Gibco, Invitrogen). The cells used for the production of the 3D ECMs were pre-conditioned to decrease their contact inhibition by culturing them for 20 passages as described in other studies.[20,49] When needed, the cells were stained with the membrane-binding dye DiD (Molecular Probes, Invitrogen).

Production and seeding of 3D cell-derived ECM scaffolds

In order to prevent the cell-derived ECMs from detaching, glass surfaces were covalently functionalized with unlabeled Fn. 8-Well chambered coverglasses (Lab-Tek, Nalge Nunc) were treated with air plasma (PDC-32G, Harrick Scientific) at 250 mbar for 30 s. The surfaces were then treated with 2% 3-aminopropyldimethylmethoxysilane (ACROS Organics) in deionized water for 15 min. The surfaces were then incubated with 0.125% glutaraldehyde (Sigma-Aldrich) in water for 30 min. Finally, the surfaces were incubated with 20 μg ml^{-1} unlabeled Fn for 1 h at room temperature or overnight at 4 °C. The chambers were sterilized by UV irradiation for 15 min.

The cell-derived ECM procedure is based on previously published protocols.[49,56,66] Cells were seeded on the prepared surfaces at 80 × 10^3 cells cm^{-2} and were allowed to attach for 30 min in the incubator; then the medium was replaced with medium containing 50 μg ml^{-1} Fn. The cells were incubated for four days, with one medium exchange after two days. On day four, the samples were washed twice with PBS, then three times with (0.1 M Na_2HPO_4, 2 mM $MgCl_2$, 2 mM EGTA, in water, pH 9.6). The samples were then incubated with lysis buffer (0.5 M Na_2HPO_4, 1% Triton X-100, pH 9.6) at 37 °C. After 15 min, the lysis buffer was exchanged and the samples were incubated at 37 °C for 1 h. The samples were rinsed twice with (10 mM Na_2HPO_4, 0.3 M KCl, in water, pH 7.5), three times with deionized water, and once with PBS. Chemical crosslinking was performed immediately after de-cellularization. Matrices were incubated with 4% formaldehyde for 1 h at room temperature. The matrices were then washed four times with PBS and incubated for 3 h in PBS before cell reseeding.

Cell-derived ECMs were reseeded with 50 × 10^3 cells cm^{-2} for FRET experiments or with 6.25 × 10^3 cells cm^{-2} for time-lapse experiments and incubated for 30 min in the incubator; then the medium was replaced with medium containing 50 μg ml^{-1} Fn. For inhibition of extracellular proteolysis, the sample medium additionally contained 20 μM Ilomastat (Chemicon, GM6001) and a 1 : 400 dilution of a protease inhibitor cocktail (Sigma, P1860) containing Bestatin, Leupeptin, Aprotinin, Pepstatin and E64. An equivalent volume of DMSO was used as a vehicle control.

Cell seeding and matrix production on manually deposited fibers

Fn fibers containing Fn-633 were manually deposited on silicone sheets either parallel or perpendicular to the direction of strain, and strained as described in the main text. The samples were blocked in 2% BSA for 1 h at room temperature. Cells were seeded onto the samples and incubated for 15 min to allow them to attach, then rinsed with medium to remove unbound cells. The samples were incubated for 30 min; then the medium was replaced with medium containing 2% BSA, 45 μg ml^{-1} unlabeled Fn and 5 μg ml^{-1} Fn-DA. The samples were cultured for 18 h, then fixed with 4% formaldehyde and imaged.

Confocal microscopy

Z-stack images were acquired with an Olympus FV1000 confocal microscope with an oil-immersion 1.35NA 60× objective. Our basic acquisition procedures for FRET imaging have been described previously.[37] For time-lapse microscopy, the confocal microscope was fitted with temperature and CO_2 control chambers (Life Imaging Services, Switzerland) that maintained the entire microscope at 37 °C, and saturated the sample with humidified air containing 5% CO_2. Images were taken every 20–30 min. for approximately 16 h.

FRET Analysis

The acceptor and donor images were analyzed using MATLAB (MathWorks, Inc.) as previously described.[37] Briefly, after correcting for the background noise and differences in

the scaling of the PMTs, the acceptor intensities were divided, pixel-by-pixel, by the donor intensities to yield the intensity ratio. All z-slices were processed individually.

Glass surfaces functionalized with silane and glutaraldehyde had a high background fluorescence that skewed the FRET ratios of fibers within about 2 μm of the surface to higher values. In the absence of surface functionalization, all z-slices in a z-stack had approximately the same intensity ratio distribution. Therefore, slices near the functionalized glass surface that showed an increase of more than 0.01 intensity ratio units were automatically detected and removed from further analysis.

Some images from four-day ECMs were contaminated with signal from endocytosed fluorescently labeled Fn that appeared in small, round vesicles as previously observed.[76] The FRET ratio of endocytosed Fn-DA centered near 0.2 and was well-separated from that of matrix fibers. Large regions of the contaminating signal were removed directly from the images by hand. Histograms of the data from images thus corrected were not significantly different from histograms of compiled data from images of similar samples not containing endocytosed Fn-DA signal.

The crosslinked scaffolds contained small (<3 μm) particulate debris that adsorbed Fn-DA, and contaminated the 18 and 48 h reseeded FRET images. Spots that had an area <100 pixels were automatically removed from these images. This algorithm had no significant effect on the median intensity ratio when applied to FRET images of matrix without particulate debris. All of these corrections were only implemented for data analysis; the images shown in this paper were not altered.

Statistical analysis

Statistical analyses were performed with MATLAB (MathWorks, Inc.) and SPSS (SPSS, Inc.). Percent unfolding and median intensity ratios for the cell-derived ECM scaffold experiments were compared using a one-way ANOVA, followed by Tukey's multi-comparison test. Unless otherwise stated, errors and error bars indicate standard deviation.

Insight, innovation, integration

Cell and tissue fate is intimately linked to the biochemistry and physical properties of their microenvironments (including mesenchyme, stroma and stem cell niches), yet no tools were available to probe how cell-generated tensile forces physically alter the properties of 3D extracellular matrix. FRET-labeled fibronectin is exploited as a mechanical strain sensor to monitor time-dependent changes of either tissue-mimetic 3D, ECM scaffolds reseeded with cells or of the newly assembled matrix fibrils. This *in situ* method is versatile, since cells, provided exogenously with FRET-fibronectin, typically co-assembled it into their ECM fibers. Probing how environmental conditions regulate cell-mediated stretching of ECM fibers is physiologically significant because stretching alters fiber rigidity and the presentation of molecular and cellular recognition sites (mechanotransduction).

Supplementary Material

Refer to Web version on PubMed Central for supplementary material.

Acknowledgments

We thank Sheila Luna for designing the cartoon in Fig. 5b, assistance with rendering the 3D reconstructions in Fig. 1, and the isolation of Fn. We also thank Li Bojun for measuring the silicone sheet stiffness. This project was

financially supported as part of the Nanotechnology Center for Mechanics in Regenerative Medicine (an NIH Roadmap Nanomedicine Development Center), the Volkswagen Stiftung, and the ETH Zurich. MLS was funded by the Human Frontier Science Program Organization.

Abbreviations

Fn	Fibronectin
Fn-DA	Doubly-labeled fibronectin
FRET	Fluorescence resonance energy transfer
GdnHCl	Guanidine HCl
MEMS	Microelectromechanical system

References

1. Bissell MJ, Inman J, Yamada KM. Reprogramming stem cells is a microenvironmental task. Proc Natl Acad Sci U S A. 2008; 105:15637–15638. [PubMed: 18843110]
2. Even-Ram S, Artym V, Yamada KM. Matrix Control of Stem Cell Fate. Cell. 2006; 126:645. [PubMed: 16923382]
3. Vessella RL, Pantel K, Mohla S. Tumor Cell Dormancy: An NCI Workshop Report. Cancer Biol Ther. 2007; 6:1496–1504. [PubMed: 17881897]
4. Engler AJ, Sen S, Sweeney HL, Discher DE. Matrix Elasticity Directs Stem Cell Lineage Specification. Cell. 2006; 126:677. [PubMed: 16923388]
5. Paszek MJ, Zahir N, Johnson KR, Lakins JN, Rozenberg GI, Gefen A, Reinhart-King CA, Margulies SS, Dembo M, Boettiger D, Hammer DA, Weaver VM. Tensional homeostasis and the malignant phenotype. Cancer Cell. 2005; 8:241–254. [PubMed: 16169468]
6. Castelló-Cros R, Khan DR, Simons J, Valianou M, Cukierman E. Staged stromal extracellular 3D matrices differentially regulate breast cancer cell responses through PI3K and beta1-integrins. BMC Cancer. 2009; 9:94. [PubMed: 19323811]
7. Chen XD, Dusevich V, Feng JQ, Manolagas SC, Jilka RL. Extracellular matrix made by bone marrow cells facilitates expansion of marrow-derived mesenchymal progenitor cells and prevents their differentiation into osteoblasts. J Bone Miner Res. 2007; 22:1943–1956. [PubMed: 17680726]
8. Yamada KM, Cukierman E. Modeling TissueMorphogenesis and Cancer in 3D. Cell. 2007; 130:601. [PubMed: 17719539]
9. Griffith LG, Swartz MA. Capturing complex 3D tissue physiology in vitro. Nat Rev Mol Cell Biol. 2006; 7:211–224. [PubMed: 16496023]
10. Wilson A, Trumpp A. Bone-marrow haematopoietic-stem- cell niches. Nat Rev Immunol. 2006; 6:93. [PubMed: 16491134]
11. Badylak SF. Xenogeneic extracellular matrix as a scaffold for tissue reconstruction. Transplant Immunol. 2004; 12:367–377.
12. Ott HC, Matthiesen TS, Goh S-K, Black LD, Kren SM, Neto TI, Taylor DA. Perfusion-decellularized matrix: using nature's platform to engineer a bioartificial heart. Nat Med. 2008; 14:213–221. [PubMed: 18193059]
13. Levy RJ, Schoen FJ, Sherman FS, Nichols J, Hawley MA, Lund SA. Calcification Of Subcutaneously Implanted Type-I Collagen Sponges-Effects Of Formaldehyde And Glutaraldehyde Pretreatments. Am J Pathol. 1986; 122:71–82. [PubMed: 3079959]
14. Valentin JE, Badylak JS, McCabe GP, Badylak SF. Extracellular Matrix Bioscaffolds for Orthopaedic Applications. A Comparative Histologic Study. J Bone Joint Surg Am. 2006; 88:2673–2686. [PubMed: 17142418]
15. Griffin M, Casadio R, Bergamini CM. Transglutaminases: Nature's biological glues. Biochem J. 2002; 368:377–396. [PubMed: 12366374]
16. Cooper ME. Importance of advanced glycation end products in diabetes-associated cardiovascular and renal disease. Am J Hypertens. 2004; 17:S31.

17. Brownlee M, Cerami A, Vlassara H. Advanced Glycosylation End Products In Tissue And The Biochemical Basis Of Diabetic Complications. N Engl J Med. 1988; 318:1315–1321. [PubMed: 3283558]

18. Smith-Mungo LI, Kagan HM. Lysyl oxidase: properties, regulation and multiple functions in biology. Matrix Biol. 1998; 16:387–98. [PubMed: 9524359]

19. Benya PD, Shaffer JD. Dedifferentiated Chondrocytes Reexpress The Differentiated Collagen Phenotype When Cultured In Agarose Gels. Cell. 1982; 30:215–224. [PubMed: 7127471]

20. Amatangelo MD, Bassi DE, Klein-Szanto AJP, Cukierman E. Stroma-Derived Three-Dimensional Matrices Are Necessary and Sufficient to Promote DesmoplasticDifferentiation of Normal Fibroblasts. Am J Pathol. 2005; 167:475–488. [PubMed: 16049333]

21. Mintz B, Illmensee K. Normal genetically mosaic mice produced from malignant teratocarcinoma cells. Proc Natl Acad Sci U S A. 1975; 72:3585–3589. [PubMed: 1059147]

22. Karnoub AE, Dash AB, Vo AP, Sullivan A, Brooks MW, Bell GW, Richardson AL, Polyak K, Tubo R, Weinberg RA. Mesenchymal stem cells within tumour stroma promote breast cancer metastasis. Nature. 2007; 449:557. [PubMed: 17914389]

23. McBeath R, Pirone DM, Nelson CM, Bhadriraju K, Chen CS. Cell shape, cytoskeletal tension, and RhoA regulate stem cell lineage commitment. Dev Cell. 2004; 6:483–495. [PubMed: 15068789]

24. Discher DE, Janmey P, Wang YL. Tissue cells feel and respond to the stiffness of their substrate. Science. 2005; 310:1139–1143. [PubMed: 16293750]

25. Vogel V, Sheetz M. Local force and geometry sensing regulate cell functions. Nat Rev Mol Cell Biol. 2006; 7:265. [PubMed: 16607289]

26. Biggs MJ, Richards RG, Gadegaard N, McMurray RJ, Affrossman S, Wilkinson CD, Oreffo RO, Dalby MJ. Interactions with nanoscale topography: adhesion quantification and signal transduction in cells of osteogenic and multipotent lineage. J Biomed Mater Res, Part A. 2009; 91:195–208.

27. Arnold M, Cavalcanti-Adam EA, Glass R, Blummel J, Eck W, Kantlehner M, Kessler H, Spatz JP. Activation of Integrin Function by Nanopatterned Adhesive Interfaces. ChemPhysChem. 2004; 5:383–388. [PubMed: 15067875]

28. Huang S, Ingber DE. Cell tension, matrix mechanics, and cancer development. Cancer Cell. 2005; 8:175–176. [PubMed: 16169461]

29. Keselowsky BG, Collard DM, Garcia AJ. Integrin binding specificity regulates biomaterial surface chemistry effects on cell differentiation. Proc Natl Acad Sci U S A. 2005; 102:5953–5957. [PubMed: 15827122]

30. Garcia AJ, Vega MD, Boettiger D. Modulation of Cell Proliferation and Differentiation through Substrate-dependent Changes in Fibronectin Conformation. Mol Biol Cell. 1999; 10:785–798. [PubMed: 10069818]

31. Bissell MJ, Hall HG, Parry G. How Does The Extracellular-Matrix Direct Gene-Expression. J Theor Biol. 1982; 99:31–68. [PubMed: 6892044]

32. Tan JL, Tien J, Pirone DM, Gray DS, Bhadriraju K, Chen CS. Cells lying on a bed of microneedles: An approach to isolate mechanical force. Proc Natl Acad Sci U S A. 2003; 100:1484–1489. [PubMed: 12552122]

33. Balaban NQ, Schwarz US, Riveline D, Goichberg P, Tzur G, Sabanay I, Mahalu D, Safran S, Bershadsky A, Addadi L, Geiger B. Force and focal adhesion assembly: a close relationship studied using elastic micropatterned substrates. Nat Cell Biol. 2001; 3:466–72. [PubMed: 11331874]

34. Engler AJ, Chan M, Boettiger D, Schwarzbauer JE. A novel mode of cell detachment from fibrillar fibronectin matrix under shear. J Cell Sci. 2009; 122:1647–53. [PubMed: 19401337]

35. Engler AJ, Richert L, Wong JY, Picart C, Discher DE. Surface probe measurements of the elasticity of sectioned tissue, thin gels and polyelectrolyte multilayer films: Correlations between substrate stiffness and cell adhesion. Surf Sci. 2004; 570:142–154.

36. Baneyx G, Baugh L, Vogel V. Coexisting conformations of fibronectin in cell culture imaged using fluorescence resonance energy transfer. Proc Natl Acad Sci U S A. 2001; 98:14464–14468. [PubMed: 11717404]

37. Smith ML, Gourdon D, Little WC, Kubow KE, Eguiluz RA, Luna-Morris S, Vogel V. Force-induced unfolding of fibronectin in the extracellular matrix of living cells. PLoS Biol. 2007; 5:e268. [PubMed: 17914904]
38. Little WC, Smith ML, Ebneter U, Vogel V. Assay to mechanically tune and optically probe fibrillar fibronectin conformations from fully relaxed to breakage. Matrix Biol. 2008; 27:451–461. [PubMed: 18417335]
39. Ohashi T, Kiehart DP, Erickson HP. Dynamics and elasticity of the fibronectin matrix in living cell culture visualized by fibronectin-green fluorescent protein. Proc Natl Acad Sci U S A. 1999; 96:2153–2158. [PubMed: 10051610]
40. Sivakumar P, Czirok A, Rongish BJ, Divakara VP, Wang YP, Dallas SL. New insights into extracellular matrix assembly and reorganization from dynamic imaging of extracellular matrix proteins in living osteoblasts. J Cell Sci. 2006; 119:1350–1360. [PubMed: 16537652]
41. Baneyx G, Baugh L, Vogel V. Supramolecular Chemistry And Self-assembly Special Feature: Fibronectin extension and unfolding within cell matrix fibrils controlled by cytoskeletal tension. Proc Natl Acad Sci U S A. 2002; 99:5139–5143. [PubMed: 11959962]
42. Antia M, Baneyx G, Kubow KE, Vogel V. Fibronectin in aging extracellular matrix fibrils is progressively unfolded by cells and elicits an enhanced rigidity response. Faraday Discuss. 2008; 139:229–249. [PubMed: 19048998]
43. Sawada Y, Tamada M, Dubin-Thaler BJ, Cherniavskaya O, Sakai R, Tanaka S, Sheetz MP. Force Sensing by Mechanical Extension of the Src Family Kinase Substrate p130Cas. Cell. 2006; 127:1015. [PubMed: 17129785]
44. del Rio A, Perez-Jimenez R, Liu R, Roca-Cusachs P, Fernandez J, Sheetz M. Stretching Single Talin Rod Molecules Activates Vinculin Binding. Science. 2009; 323:638–641. [PubMed: 19179532]
45. Hocking DC, Titus PA, Sumagin R, Sarelius IH. Extracellular Matrix Fibronectin Mechanically Couples Skeletal Muscle Contraction with Local Vasodilation. Circ Res. 2008; 102:372–379. [PubMed: 18032733]
46. Zhong C, Chrzanowska-Wodnicka M, Brown J, Shaub A, Belkin AM, Burridge K. Rho-mediated Contractility Exposes a Cryptic Site in Fibronectin and Induces Fibronectin Matrix Assembly. J Cell Biol. 1998; 141:539–551. [PubMed: 9548730]
47. Vogel V. Mechanotransduction involving Multimodular Proteins: Converting Force into Biochemical Signals. Annu Rev Biophys Biomol Struct. 2006; 35:459–488. [PubMed: 16689645]
48. Vogel V, Sheetz MP. Cell fate regulation by coupling mechanical cycles to biochemical signaling pathways. Curr Opin Cell Biol. 2009; 21:38–46. [PubMed: 19217273]
49. Cukierman E, Pankov R, Stevens DR, Yamada KM. Taking Cell-Matrix Adhesions to the Third Dimension. Science. 2001; 294:1708–1712. [PubMed: 11721053]
50. Beningo KA, Dembo M, Wang Y-l. Responses of fibroblasts to anchorage of dorsal extracellular matrix receptors. Proc Natl Acad Sci U S A. 2004; 101:18024–18029. [PubMed: 15601776]
51. Grinnell F. Fibroblasts, myofibroblasts, and wound contraction. J Cell Biol. 1994; 124:401–404. [PubMed: 8106541]
52. Doyle AD, Wang FW, Matsumoto K, Yamada KM. One-dimensional topography underlies three-dimensional fibrillar cell migration. J Cell Biol. 2009; 184:481–490. [PubMed: 19221195]
53. Zaman MH, Trapani LM, Sieminski AL, MacKellar D, Gong H, Kamm RD, Wells A, Lauffenburger DA, Matsudaira P. Migration of tumor cells in 3D matrices is governed by matrix stiffness along with cell-matrix adhesion and proteolysis. Proc Natl Acad Sci U S A. 2006; 103:10889–10894. [PubMed: 16832052]
54. Meshel AS, Wei Q, Adelstein RS, Sheetz MP. Basic mechanism of three-dimensional collagen fibre transport by fibroblasts. Nat Cell Biol. 2005; 7:157. [PubMed: 15654332]
55. Klotzsch E, Smith ML, Kubow KE, Muntwyler S, Little WC, Beyeler F, Gourdon D, Nelson BJ, Vogel V. Fibronectin forms the most extensible biological fibers displaying switchable force-exposed cryptic binding sites. Proc Natl Acad Sci U S A. 200910.1073/pnas.0907518106
56. Mao Y, Schwarzbauer JE. Stimulatory effects of a three-dimensional microenvironment on cell-mediated fibronectin fibrillogenesis. J Cell Sci. 2005; 118:4427–4436. [PubMed: 16159961]

57. Mao Y, Schwarzbauer J. Accessibility to the Fibronectin Synergy Site in a 3DMatrix Regulates Engagement of alpha5beta1 versus alphaVbeta3 Integrin Receptors. Cell Commun Adhes. 2006; 13:267. [PubMed: 17162669]
58. Badylak SF, Freytes DO, Gilbert TW. Extracellular matrix as a biological scaffold material: Structure and function. Acta Biomater. 2009; 5:1–13. [PubMed: 18938117]
59. Wolf K, Mazo I, Leung H, Engelke K, von Andrian UH, Deryugina EI, Strongin AY, Brocker EB, Friedl P. Compensation mechanism in tumor cell migration: mesenchymal-amoeboid transition after blocking of pericellular proteolysis. J Cell Biol. 2003; 160:267–277. [PubMed: 12527751]
60. Jiang G, Giannone G, Critchley DR, Fukumoto E, Sheetz MP. Two-piconewton slip bond between fibronectin and the cytoskeleton depends on talin. Nature. 2003; 424:334. [PubMed: 12867986]
61. Petroll MW, Ma L. Direct, dynamic assessment of cell-matrix interactions inside fibrillar collagen lattices. Cell Motil Cytoskeleton. 2003; 55:254–264. [PubMed: 12845599]
62. Vogel V, Baneyx G. The Tissue Engineering Puzzle: A Molecular Perspective. Annu Rev Biomed Eng. 2003; 5:441–463. [PubMed: 14527318]
63. Yeung T, Georges PC, Flanagan LA, Marg B, Ortiz M, Funaki M, Zahir N, Ming W, Weaver V, Janmey PA. Effects of substrate stiffness on cell morphology, cytoskeletal structure, and adhesion. Cell Motil Cytoskeleton. 2005; 60:24–34. [PubMed: 15573414]
64. Sun Y, Wan KT, Roberts KP, Bischof JC, Nelson BJ. Mechanical property characterization of mouse zona pellucida. IEEE Trans NanoBiosci. 2003; 2:279–286.
65. Ulmer J, Geiger B, Spatz JP. Force-induced fibronectin fibrillogenesis in vitro. Soft Matter. 2008; 4:1998–2007.
66. Chen LB, Murray A, Segal RA, Bushnell A, Walsh ML. Studies on Intercellular LETS Glycoprotein Matrices. Cell. 1978; 14:377–391. [PubMed: 667946]
67. Bershadsky A, Balaban NQ, Geiger B. Adhesion-dependent cell mechanosensitivity. Annu Rev Cell Dev Biol. 2003; 19:677–695. [PubMed: 14570586]
68. Christopher R, Kowalczyk A, McKeown-Longo P. Localization of fibronectin matrix assembly sites on fibroblasts and endothelial cells. J Cell Sci. 1997; 110:569–581. [PubMed: 9092939]
69. Solon J, Levental I, Sengupta K, Georges PC, Janmey PA. Fibroblast adaptation and stiffness matching to soft elastic substrates. Biophys J. 2007; 93:4453–4461. [PubMed: 18045965]
70. Ruiz SA, Chen CS. Emergence of Patterned Stem Cell Differentiation within Multicellular Structures. Stem Cells. 2008; 26:2921–2927. [PubMed: 18703661]
71. Baneyx G, Vogel V. Self-assembly of fibronectin into fibrillar networks underneath dipalmitoyl phosphatidylcholine monolayers:role of lipid matrix and tensile forces. Proc Natl Acad Sci U S A. 1999; 96:12518–23. [PubMed: 10535954]
72. Krammer A, Craig D, Thomas WE, Schulten K, Vogel V. A structural model for force regulated integrin binding to fibronectin's RGD-synergy site. Matrix Biol. 2002; 21:139–147. [PubMed: 11852230]
73. Lan MA, Gersbach CA, Michael KE, Keselowsky BG, Garcia AJ. Myoblast proliferation and differentiation on fibronectin-coated self assembled monolayers presenting different surface chemistries. Biomaterials. 2005; 26:4523. [PubMed: 15722121]
74. Butcher DT, Alliston T, Weaver VM. A tense situation: forcing tumour progression. Nat Rev Cancer. 2009; 9:108. [PubMed: 19165226]
75. Tomasek JJ, Gabbiani G, Hinz B, Chaponnier C, Brown RA. Myofibroblasts and mechanoregulation of connective tissue remodelling. Nat Rev Mol Cell Biol. 2002; 3:349–363. [PubMed: 11988769]
76. Sottile J, Chandler J. Fibronectin Matrix Turnover Occurs through a Caveolin-1 Dependent Process. Mol Biol Cell. 2005; 16:757–768. [PubMed: 15563605]

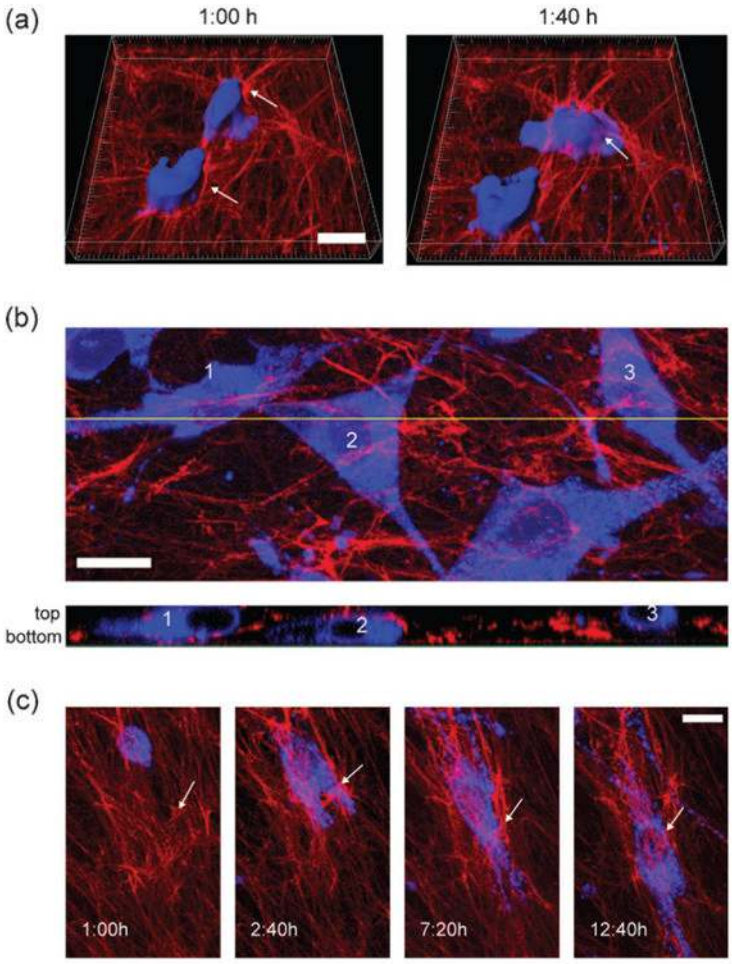

Fig. 1.

Fiber rearrangements in the ECM scaffold caused by fibroblast invasion and migration. Membrane-stained fibroblasts (blue) were seeded into native de-cellularized ECM scaffolds containing fluorescently labeled Fn (red). All times are relative to the time of seeding. The gamma settings for the images have been modified in order to achieve a more even fluorescence. All bars are 20 μm. (a) 3D reconstructions of two fibroblasts invading a scaffold at 1:00 and 1:40 h after seeding. 1:00: both cells have penetrated the scaffold by pushing the fibers out of the way, leading to the formation of a ring of compacted fibers (arrows). 1:40: both cells have begun to polarize, causing the hole to change shape and one cell has pulled fibers over its dorsal surface (arrow). (b) Z-projection image (top) and profile (taken at yellow line in the top image) 16 h after reseeding. See main text for description. Cells in crosslinked scaffolds appeared similar. (c) Frames from Supplementary Movie 1[†] showing a migrating cell encountering fibers perpendicular to its path (arrows). 1:00: the original state of the obstructing fibers. 2:40–7:20: the pseudopodia pull fibers backward while the bulky cell body pushes the obstructing fibers forward resulting in fiber compaction and large fiber rearrangements. 12:40: the obstructing fibers finally pass of the cell's nucleus.

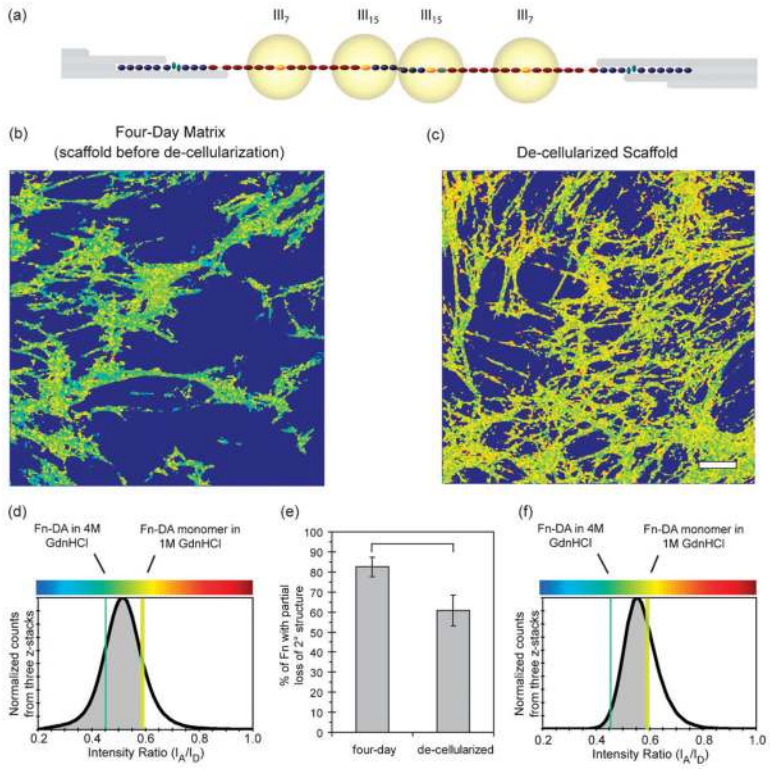

Fig. 2.

De-cellularization of four-day old matrices reverted Fn unfolding as probed by FRET. (a) To-scale cartoon of a Fn dimer showing placement of the acceptor dyes on residues $FnIII_7$ and $FnIII_{15}$, and the 6 nm radius of energy transfer. Donors are conjugated randomly to lysines and thus, exact locations are not depicted. Representative intensity ratio measurements of the cell-derived ECM are shown before (b,d) and after (c,f) de-cellularization. The two images are single z-slices from the specified sample, color-coded by intensity ratio (see color bar). The histograms show the distribution of intensity ratios compiled from three experiments (three z-stacks each). The 1 M and 4 M GdnHCl denaturation points (ESI, Fig. S1[†]), are indicated with the colored lines. The shaded areas under the histograms show the portion of the population that has partial loss of secondary structure (*i.e.* intensity ratios less than the 1Mmonomer point). (d) The unfolded populations are expressed as percentages mean ± s.d.). The bracket indicates $p < 0.05$ ($N = 5$ (four-day), 3 (de-cellularized)). Bar is 20 μm.

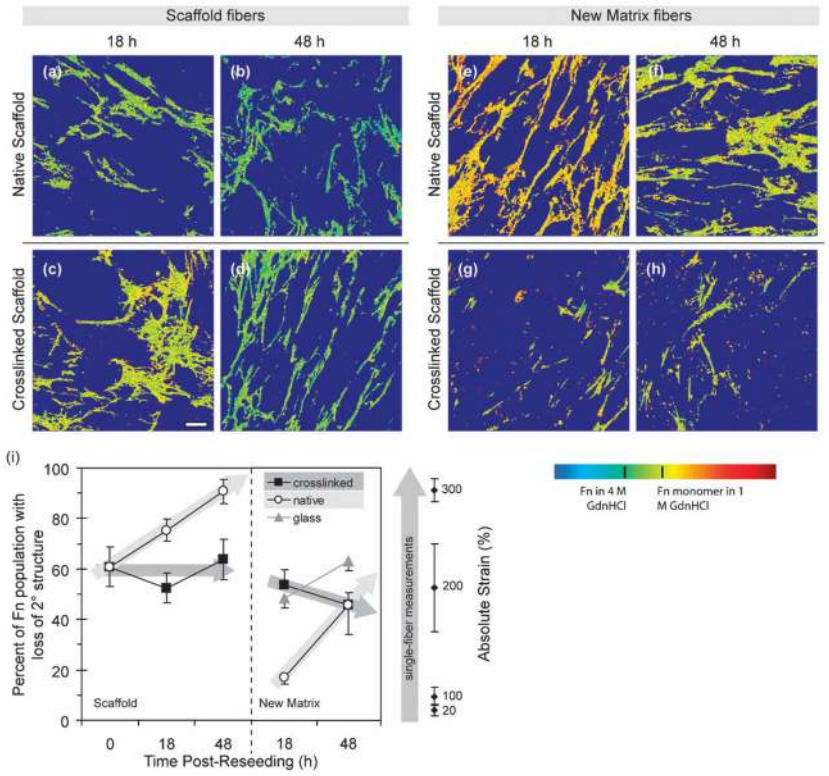

Fig. 3.

Progressive Fn stretching and unfolding trends in the native and crosslinked scaffolds, and in newly deposited matrix (lower panels) caused by cell generated traction forces. Representative z-slices, depicted as in Fig. 2. See Fig. 2c for the de-cellularized scaffold prior to reseeding (t =0). (a–d) The native and crosslinked scaffolds and (e–h) the newly deposited matrix 18 and 48 h after reseeding. Corresponding histograms can be found in the ESI, Fig. S2.† (i) The percentage of the Fn populations with loss of secondary structure as defined in Fig. 2 is shown for the native (white circles) and crosslinked (black squares) scaffolds' fibers and the new matrix fibers. Data for ECM fibers deposited by cells directly seeded onto glass are shown for comparison (gray triangles). The axis labels on the right side of the plot show approximate strains of single Fn fibers that correspond to different levels of unfolding (mean ± s.d.) and is summarized from ref. [55]. Bar is 20 μm.

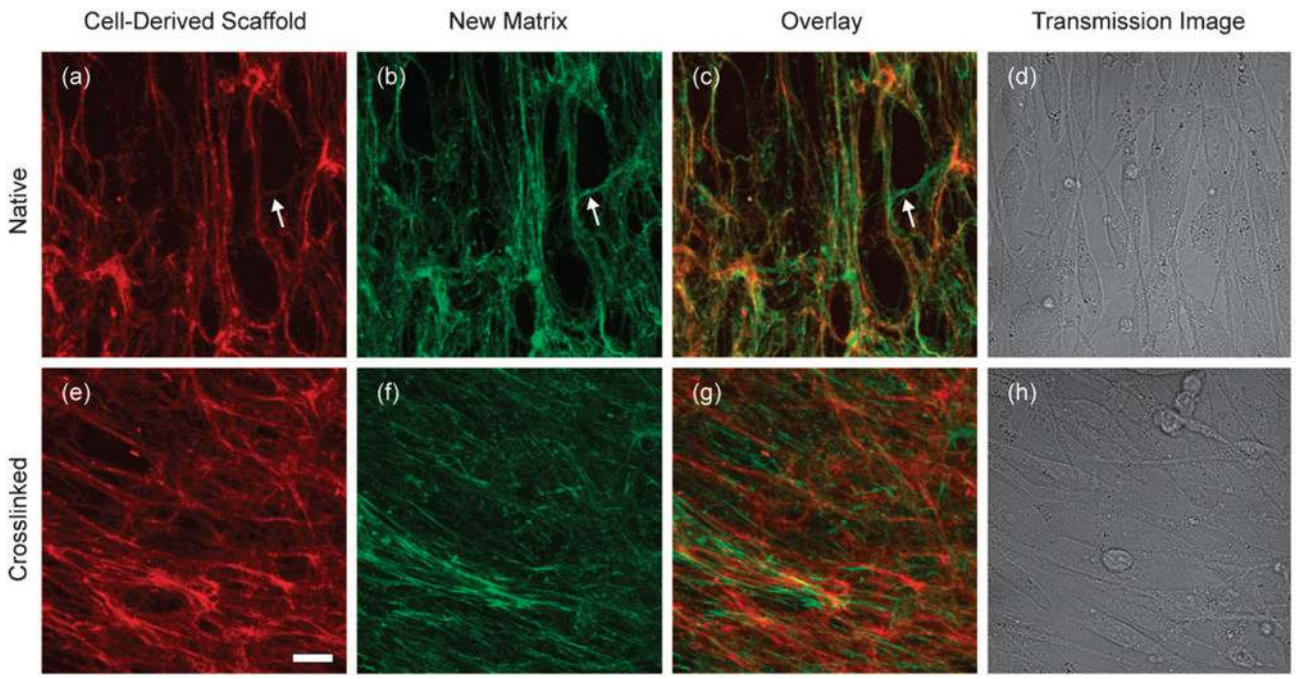

Fig. 4.

Morphology of the new matrix deposited by cells in native and crosslinked scaffolds. Fluorescence z-stack projections of the scaffold (red), new matrix fibers (green) and overlay along with a transmission image for the same field-of-view in native and crosslinked scaffolds 48 h after reseeding. New fibers in the native scaffold are mostly highly localized to the scaffold's fibers but there are also independent fibers (a, b, c, arrows). In contrast, new fibers in the crosslinked scaffolds do not co-localize with the existing fibers, although they are aligned in the same general direction. The images are representative of three independent experiments. Bar is 20 μm.

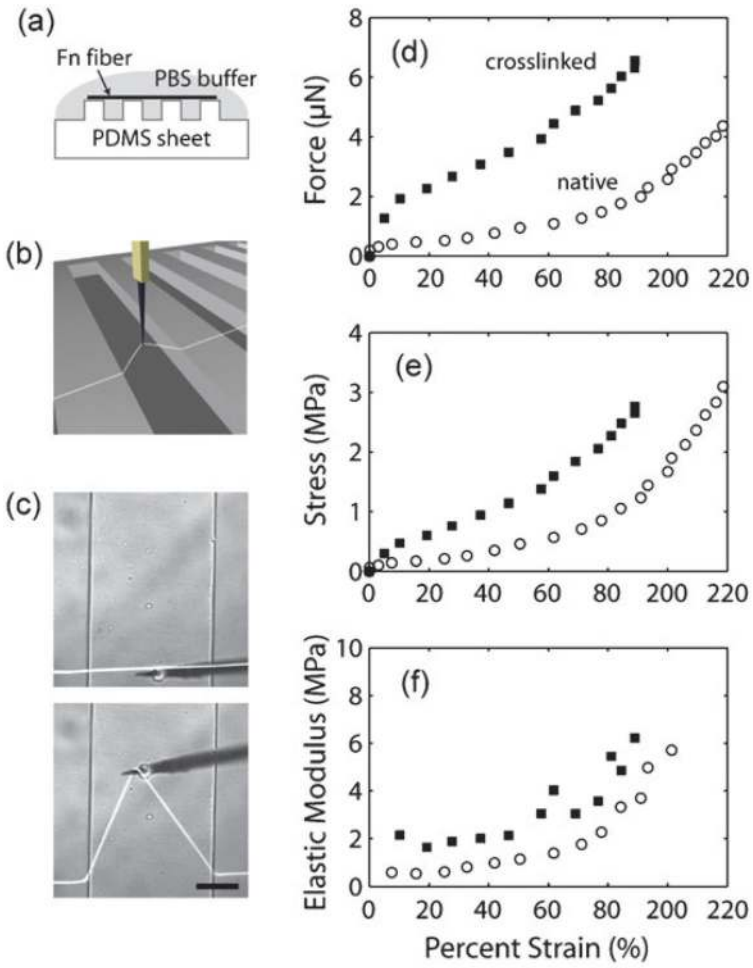

Fig. 5.

Chemical crosslinking increases Fn fiber rigidity. (a) Manually deposited Fn fibers were suspended over PDMS ridges and immersed in PBS. (b) The suspended section of the fiber was strained using a MEMS probe. (c) A top-down fluorescence and DIC image overlay of a Fn fiber (fluorescently labeled), before and after being stretched to 200% strain. Bar is 50 μm. (d–f) Representative data for one fiber, measured before (open circles) and after (filled squares) crosslinking; data for additional fibers can be found in the ESI, Fig. S4.† The force (c), stress (d) and elastic modulus (e) are plotted as a function of percent one-dimensional strain.

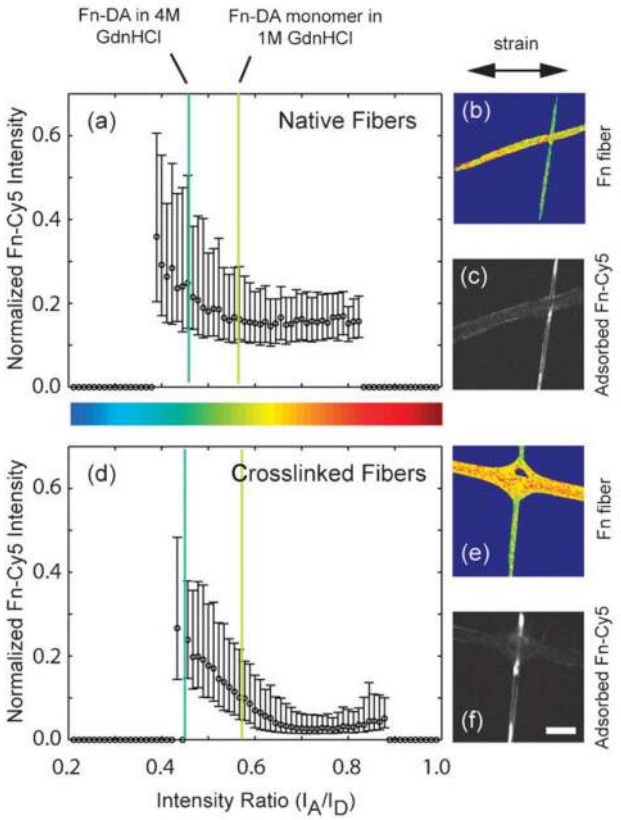

Fig. 6.

Chemical crosslinking does not alter Fn self-association binding sites. Plots (a) and (d) show the median, 25th and 75th percentiles of the intensity of Fn-Cy5 bound to Fn fibers with specific intensity ratios (binned). Because the samples were prepared separately, their normalized intensity values (on the y-axis) are not directly comparable. Fig. (b) and (e) show representative intensity ratio images of the manually deposited fibers, while (c) and (f) show the corresponding Fn-Cy5 fluorescence images. The data in (a) and (d) are from six fibers each. This experiment was repeated with similar results. Bar 20 is μm.

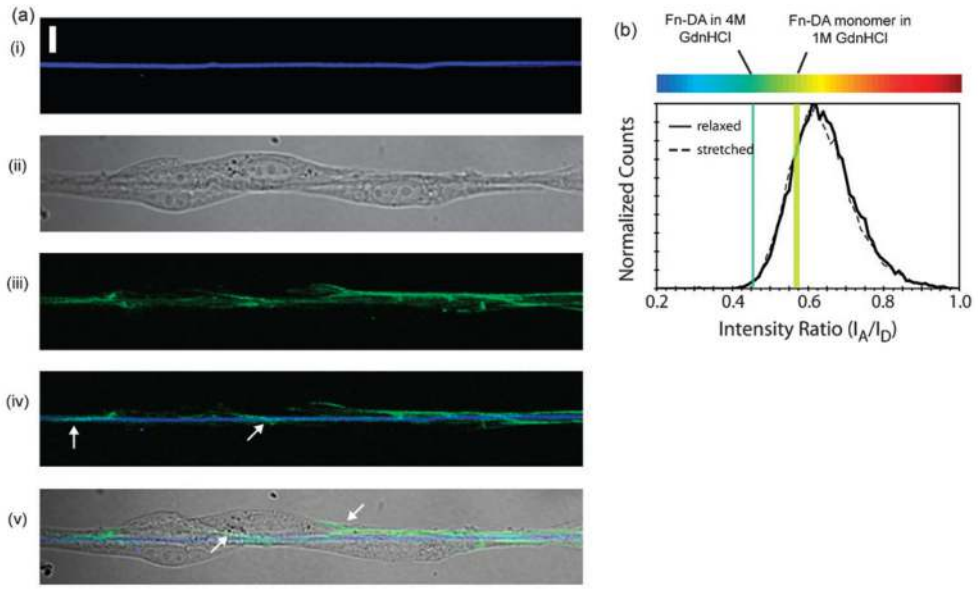

Fig. 7.

Conformation of single Fn fibers deposited on silicone sheets compared to the conformation of Fn in the ECM of cells sitting on the fibers. (A) Representative images of cells and the matrix that they deposited (green) sitting on a manually deposited fiber (blue) after 18 h. (i) Manually deposited fiber. (ii) DIC image of fibroblasts adhering to the fiber. (iii) Z-projection of the Fn matrix produced by the cells over 18 h. (iv) Overlay of the cell-generated (green) and manually deposited (blue) fibers from one z-slice, 2 μm above the surface. The arrows show locations where the cell-generated fibers attach to the manually deposited fiber. Below this slice, only the manually deposited fiber was visible. (v) Overlay of all three channels from one z-slice, 4 μm above the surface. The arrows show locations where the cell-generated fibers wrap around the cell. (B) Histogram of the intensity ratio distributions from the matrix on relaxed (solid line) and stretched (dashed line) manually deposited fibers. The Fn-DA used here is different from that used in the scaffold experiments (ESI, Fig. S1C,D†).